JOURNAL OF MATERIALS SCIENCE **35** (2000) 2061–2067

Computer experiments on nano-indentation: A molecular dynamics approach to the elasto-plastic contact of metal copper

YONGSHENG LENG*
State Key Laboratory of Tribology, Tsinghua University, Beijing 100084, People's Republic of China; Division of Mechanics, College of Architecture, North China University of Technology, Beijing 100041, People's Republic of China
E-mail: lengys@u.washington.edu

GUIPING YANG
Division of Mechanics, College of Architecture, North China University of Technology, Beijing 100041, People's Republic of China

YUANZHONG HU, LINQING ZHENG
State Key Laboratory of Tribology, Tsinghua University, Beijing 100084, People's Republic of China

Molecular dynamics simulations are used to investigate the micro-mechanisms of nano-indentation for tip to substrate contact. The method combines a many-body interatomic potential derived from the nearest-neighbor EAM and brownian dynamics (BD) approach to simulate a rigid tip indenting Cu (001) surface. Elastic contact and plastic instability of the crystal are investigated through the loading-unloading cycle, the variations of the system potential energy versus the tip approach, the atomic stress distributions and the portraits of atomic trajectories and configurations. For elastic indentation, we find that atomistic stress distributions resembling roughly to those of the continuum Hertzian fields, except for a jump-to-contact phenomenon in the initial contact stage. When the tip approach is beyond some critical value, plastic instability of the substrate occurs, and both the contact load and potential energy decrease dramatically. Detailed calculations reveal that material yield at the atomic level is still governed by the von Mises shear strain-energy criterion, while atomistic trajectories show that the displacements in (010) plane of atoms near the contact region is similar to that in Johnson's cavity model, accompanied by atomic cross-layer movements in [010] direction to release the strain energy. The crystal defects after plastic indentation include subsurface cavities, surface atomic steps and plastic indent.

1. Introduction

The behavior of solid surfaces under macroscopic and microscopic indentation have been studied intensively over the past ten years, both in experimental and theoretical aspects [1–3]. These critical investigations are directly related to the tribological performances of conventional engineering surfaces, and more recently, of those used in magnetic recording devices and microelectronics, such as smooth ultrathin films with novel microstructures. In recent years, the rapid emergence of microelectromechanical systems (MEMS) has increased the *demand for achieving submicrometer tolerances* without sacrificing the reliability of ingenious components [4]. In engineering precision cutting processes, high-tolerance parts with dimensional tolerance of a few tens of nanometers are currently being produced using advanced diamond tools [5]. In these circumstances, surface contacts or indentations may occur in grain boundaries or within a single grain, results in nano-indentation problems. It is obvious that continuum contact mechanics [6] could not be used to deal with these difficult tasks.

Molecular dynamics (MD) simulation, as a mature computer experimental approach, opens a new avenue to search for the solutions to the above mentioned nanomechanics problems. As precursors, Landman *et al.* [7] used molecular dynamics simulations and atomic force microscopy (AFM) to investigate the atomistic mechanisms of nickel tip to gold surface adhesion, nanoindentation and separation processes. Belak and Stowers [8] made MD simulations of nanometer-scale deformation of metallic and ceramic surfaces. At approximately the same time, a massive MD system composed of over one million atoms were established

* Current address: Department of Chemical Engineering, University of Washington, Box # 351750, Seattle, WA 98195-1750, USA.

to investigate the non-equilibrium indentation of two-dimensional crystals [9].

The experience of recent MD simulations in tribology field has shown that this novel approach does give significant insights into the atomic scale phenomena related to contact formation, separation and fracture of interfaces [7], friction at sliding diamond interfaces with hydrogen or methyl group terminations [10], and reduction in the adhesion force due to the presence of adsorbed film on the substrate [11]. However, from the point of view of micro/meso mechanics, a detailed microscopic picture of material failures, such as surface and near surface defects initiation and evolution mechanisms in friction and wear processes is still lacking. It is our purpose in this paper to give a complete description of the tip-to-substrate approach, which is similar to that of Landman [7] and Belak's [8] problem. However, our emphases are placed on the atomic stress analyses, load-approach and system potential energy variations and the defects generation mechanisms during the elastic-plastic contact of crystals, which have considerable practical relevance to the microhardness of ultra-thin films and the material failure modes.

We conduct MD simulations via the embedded-atom method (EAM) originally proposed by Daw and Baskes [12]. But in practice, we adopt Johnson's first neighbor modifications (FNEAM) [13] for face-centered cubic (FCC) copper to accelerate the force calculations of interacting particles. In section 2, we will give a brief description of our model system and MD simulation method. We present our MD results and analyses in section 3, followed by a summary in section 4.

2. Methodology

Our MD system is composed of a crystal copper slab with FCC structure exposing (001) surface, and interacting with a blunted rigid tip. The tip is cleaved by two (110) planes and two (001) planes from an FCC structure, which makes the tip infinitely wide in the [010] direction. The substrate contains two static bottom layers and eighteen dynamic layers with each layer consisting of 320 atoms. The total number of atoms in the substrate is 6400, while that of the tip is 140 atoms. The size of the MD cell in the y direction [001] is $9.5a_0$, where a_0 is the equilibrium lattice constant (for FCC Cu, $a_0 = 0.3615$ nm). This makes the substrate have a thickness of about 3.4 nm, which is comparable with that in nano-scale indentation hardness test of thin films [14]. The sizes of the computational cell in the x [100] and z [010] directions are $40a_0$ and $4a_0$ respectively. Periodic boundary conditions are imposed on [100] and [010] directions. In so doing, the tip-to-substrate approach in our MD system mimics a plane stain problem in the continuum elasticity.

In our previous simulations, we used the embedded-atom method (EAM) developed by Foiles *et al.* [15] to calculate the atomic potentials and forces. However, we find it is more convenient to adopt Johnson's simple nearest-neighbor analytic model [13], which to the first-order effects, takes into account the nearest neighbor contributions to the electron density and the two-body potential in the FCC lattice. In the Johnson's FNEAM, the cutoff distance is between the first and second neighbors, which makes the force calculations quite fast. Thus, in our MD simulations, this value is taken to be $0.8a_0$ conveniently.

In this study, the substrate is treated as a cold crystal slab with temperature being controlled around 0.1 K via brownian dynamics method (see below). The reason for doing this is that the fluctuations of the atomic stress distributions due to the thermal effects can be significantly decreased, and moreover, the crystal defects initiation mechanisms can be depicted clearly. However, a better understanding of the thermal effects on these problems is now being undertaken. The tip is treated rigid (the tip atoms do not evolve with the time) and moves towards the substrate with increments of $0.02a_0$ over 200 Δt, where the time step $\Delta t = 3$ fs. This corresponds to an indentation speed of 12 m/s. For perfect crystals at low temperature, the longitudinal sound speed is usually in the order of 10^3 m/s [9]. In comparison with the indentation speed of the rigid tip, our results could be recognized approximately as quasi-static in nature. Prior to indentation, the distance between the bottom layer of the tip and the topmost layer of the substrate is set to be $0.8a_0$, and the corresponding tip approach is denoted by zero.

The equations of motion of the dynamic substrate atoms are integrated using a third order Verlet algorithm for brownian dynamics (BD) [16]. Our earlier calculations with predictor-corrector Gear-4 algorithm and simple velocity rescaling [17] to control the temperature revealed that nonphysical sound waves due to the surface relaxation and tip indentation were reflected between the bottom static layers and the free surface, resulting in a non-Gaussian velocity distributions of particles in the y [001] direction. These reflecting waves can only be eliminated with the technique of stochastic approach. Within the framework of brownian dynamics (BD), the motion of atomic system is approximated by including the systematic force $F_i(\{x(t)\})$ into the ordinary Langevin equation:

$$m_i \dot{v}_i(t) = F_i(\{x(t)\}) - m_i \gamma v_i(t) + R_i(t) \qquad (1)$$

where $R_i(t)$ represents a random "white noise" force which is assumed to be stationary, Markovian and Gaussian with zero mean, and γ is a damping coefficient, its reasonable value is $\pi/6$ times the Debye frequency ω_D (for FCC Cu, $\gamma = 23{\cdot}5$ ps^{-1}) [18]. The systematic force F_i can be directly calculated from EAM potential, which may depends on the coordinates of all particles, denoted by $\{x(t)\}$. We control the system pressure using the external pressure bath method [19]. The external reference pressure p_0 is taken to be a few tens of bar (in the order of 10^{-3} GPa). In comparison with the atomic stresses during indentation, this represents a vanishingly low pressure.

The atomic stresses for the system of discrete particles can be calculated through the dynamical theory of crystal lattices by Born and Huang (1954) [20]. For

many-body potentials, the atomic level stress tensor associated with an atom α is [21]

$$\sigma_{ij}^{\alpha} = \frac{1}{\Omega^{\alpha}} \sum_{\beta(\neq\alpha)} \frac{\partial E_{\alpha}}{\partial R_i^{\alpha\beta}} R_j^{\alpha\beta} \tag{2}$$

where the summation extends over all the neighbors of atom α, E_{α} is the potential energy associated with atom α derived from FNEAM, and is a function of the vector $R^{\alpha\beta}$, separating atom α and its neighbors β. Ω^{α} is the atomic volume.

The atomic von Mises equivalent stress is

$$\sigma_{\text{eq}} = J_2^{\frac{1}{2}} \qquad J_2 = \frac{1}{2} S_{ij} S_{ij} \tag{3}$$

where S_{ij} is the deviatoric stress tensor, given by $S_{ij} = \sigma_{ij} - \frac{1}{3}\sigma_{kk}\delta_{ij}$.

3. Results and analyses

Prior to the tip approaching, we allow the substrate to have 1ps relaxation, and find that the surface energy of Cu(001) is 1.175 J/m^2, a reasonable value lower than the unrelaxed energy (= 1.20 J/m^2) [13]. The surface relaxation of the top layer spacing d_{12}, and of the second layer spacing d_{23} for (001) faces relative to the bulk interlayer spacing are -3.5% and 0.2% respectively.

3.1. Elastic indentation and retraction

Fig. 1a and b represent the variations of the contact load and system potential energy versus the tip approach, respectively. We observe that during the initial contact stage, the attractive force between the tip and the substrate increases dramatically, and the energy curve decreases sharply. This instability corresponds to the jump-to-contact (JC) Phenomenon [7]. Our simulations show that during the JC process, the kinetic temperature of the system increases from 0.1 K to 0.35 K due to the bulging of the surface atoms, then this temperature rise is dissipated to the ambiance in a time span of 1 ps through stochastic collisions. At onset of contact formation, where the tip approach is approximately $0.04a_0$, the maximum attractive force, or the adhesion force F_y attains a value of 16 nN. Fig. 2a shows an atomic (010) slice at JC stage, which portrays the bulging of the surface atoms just beneath the outmost layer of the tip. The Cu atoms in the region of the surface under the tip displace by approximately 0.15 nm toward the tip in a short time span of 0.6 ps.

As the tip approach continues to increase, the load curve starts to go up, however, the potential energy continues to drop down until it reaches a local minimum at $0.32a_0$, where the contact load equals approximately to zero. At this point, the system is stable, where the metal bonding between the tip and the substrate is constructed without bond stretching. Further indentation of the substrate by the rigid tip reveals that the contact load increases linearly with the distance, while the potential energy increases monotonically, indicating that the strain energy is stored in the strained substrate due to the interatomic interactions between the tip and the sample. The corresponding atomic configuration for tip approach being $1.3a_0$ is shown in Fig. 2b, which notably depicts the surface elastic deformation of the substrate. Here we see the topmost layer of the tip reaches the second layer position of the dynamic substrate, and the

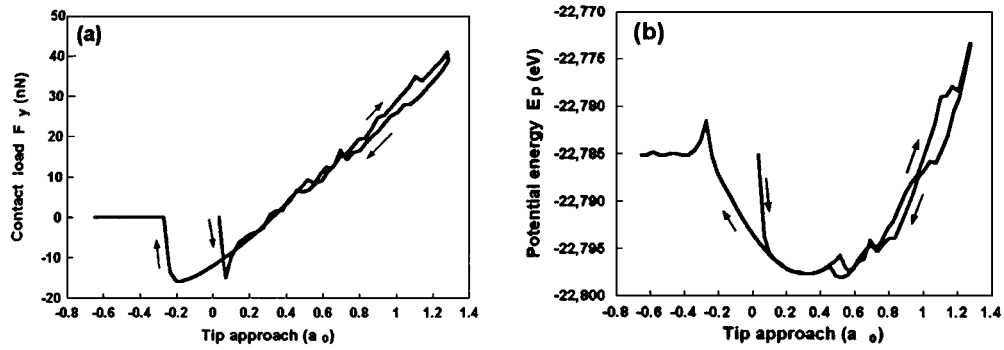

Figure 1 Variations of (a) the contact load F_y and (b) system potential energy E_p versus tip-to-substrate approach.

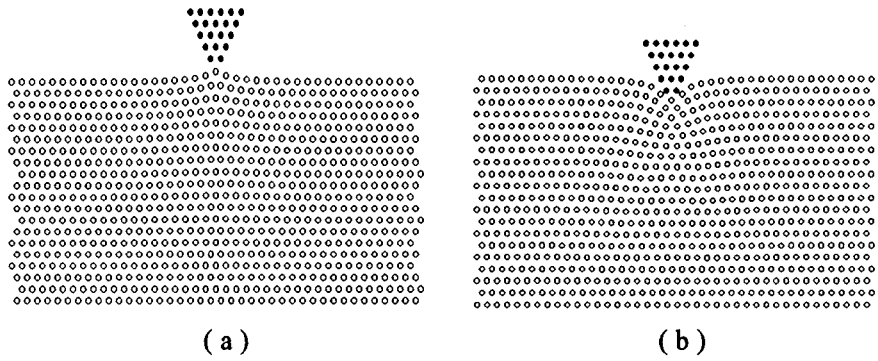

Figure 2 Atomic configurations of (a) adhesion and (b) indentation.

sample surface atoms are indented approximately to the third layer position. Upon retraction of the tip, we observe that the unloading curve is almost along the loading path, suggesting that the response of the material is linearly elastic. However, beyond the JC point, marked hysteresis occurs as a consequence of adhesive bond stretching between the two materials. This phenomenon was also observed by Landman *et al.* [7]. When the adhesion junction breaks, we do not observe the materials transfer, that is, the Cu sample atoms adhere to the Cu rigid tip. This may be due to the small difference of surface energies between the two materials, and moreover, to the low temperature of the crystal slab. The variation of the potential energy displays the same trend as that of the load—distance curve. In particular, it comes back to the primitive value after the tip separated from the sample, indicating that no adhesion defects are generated during the elastic indentation (otherwise there will be induced defect energies, see below for the plastic indentation). This can also be demonstrated from the atomic configuration after the debonding between the tip and the substrate.

In our MD simulations, the atomic stress distributions are drawn along [100] at surface and [001] on the y axis. For the elastic indentation, the stress components $\sigma_z \neq 0$, and $\tau_{zx} = \tau_{zy} = 0$, demonstrating that the contact problem is of the plane strain in nature. During the JC process and the liftoff of the tip at the hysteresis stage, we find that the normal stresses σ_x and σ_y at the surface are tensile, while the shear stress τ_{xy} is anti-symmetric due to the attraction of the tip to the side atoms. Fig. 3 is a prototype of the surface stress distributions in the hysteresis stage. It is obvious that the adhesion contact stress σ_y is much greater than the surface tensile stress σ_x, while the magnitude of the shear stress τ_{xy} is relatively lower. Detailed calculations reveal that at the JC point, σ_y attains a value of 19.5 GPa, while in the hysteresis stage, it has a maximum value of 28 GPa at the moment the contact junction breaks. This critical value is consistent with the Griffith theoretical fracture strength (30 GPa for usual metals) for Mode-I crack propagation [22]. Outside the contact region, the surface stresses σ_x, σ_y and τ_{xy} level off to 7 GPa, 3 GPa and zero, respectively. The non-zero stresses of σ_x and σ_y are due to the surface relaxation of the substrate. This phenomenon is also described in recent investigations on the Mode-I crack stress relaxation problems [23].

The atomic stress distributions along [100] at the surface and [001] on the y axis when the tip approach is

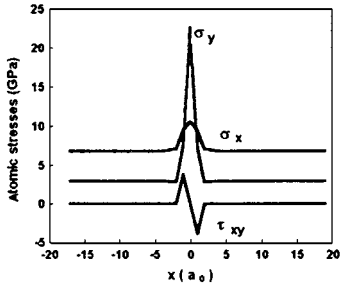

Figure 3 Atomic stress distributions along the x direction in adhesion contact.

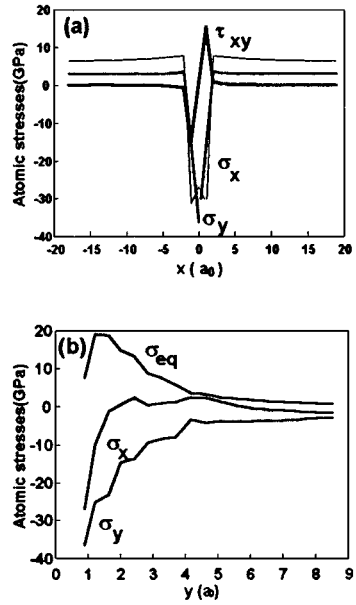

Figure 4 Atomic stress distributions along (a) x and (b) y directions in indentation contact.

$1.3a_0$ are drawn in Fig. 4a and b. In Fig. 4a, both the contact stress σ_y and the tangential normal stress σ_x are negative (compressive), while the surface shear stress τ_{xy} is still anti-symmetric and opposite to that in JC process, resembling to the near-surface shear stress distribution in the continuum contact mechanics [6]. The contact pressure distribution σ_y, could be roughly recognized as of a Hertzian type, and its maximum value is 36 GPa at the contact center. In particular, it is interesting to note that, at atomistic level, the maximum Mises equivalent stress σ_{eq} along y axis occurs at the second layer position (approximately in the depth of $0.5a_0$, see Fig. 4b), in accordance with the continuum Hertzian theory, where yield begins at a point below the surface [6]. Fig. 4b also reveals that, as the surface atoms being elastically indented into the third layer position (corresponding to the surface deformation equal to a_0), the elastic disturbance is well within the range of $8a_0$. This effects the rule-of-thumb in ultra-thin film indentation hardness tests, which states that penetration depths less than 10 to 20 percent of the layer thickness will not include substrate material influences [3].

3.2. Plastic indentation and retraction

We turn now to the material plastic instability, where yielding is driven by the release of the strain energy stored in the substrate for tip-to-substrate approach. The defects nucleation at microcontacts [24] are of significant importance to the strength of materials, and the knowledge about the voids initiation and evolution mechanisms is still lacking.

Further indentation of the rigid tip allows its outmost layer to reach the third layer position of the substrate, where the maximum tip approach is $1.8a_0$. Our findings reveal that, when the tip approach is greater than a critical value (about $1.46a_0$), both the contact load and the potential energy start to decrease (Fig. 5a and b). This phenomenon of material softening corresponds to the

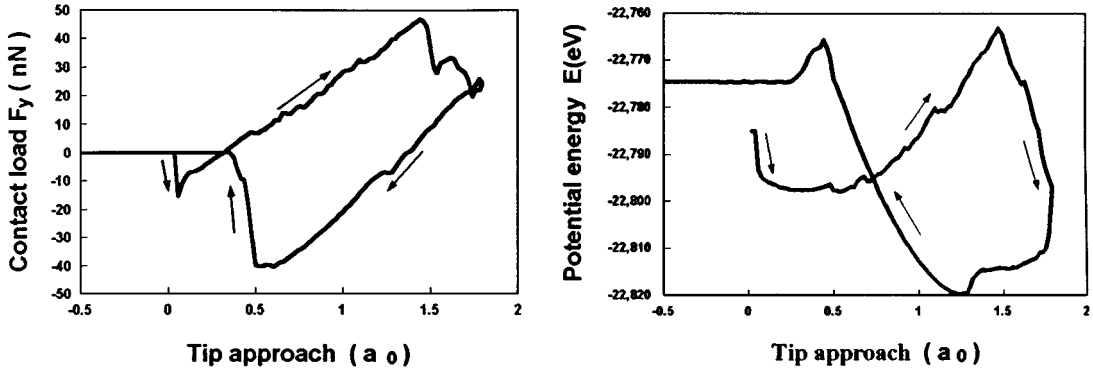

(a) (b)

Figure 5 (a) Plastic loading-unloading curve. (b) Variation of the potential energy in plastic loading-unloading cycle.

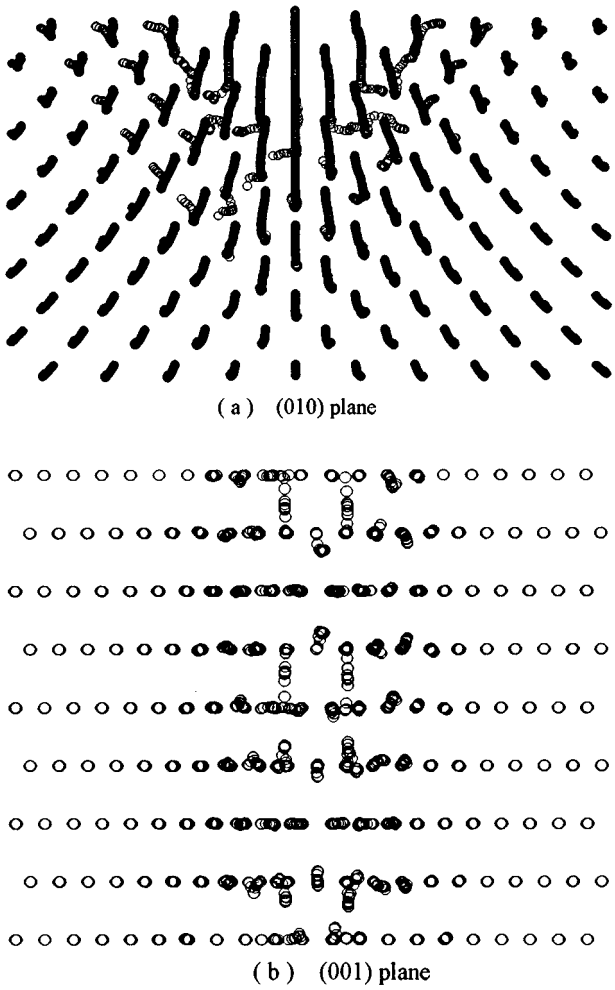

Figure 6 Atomic trajectories in plastic indentation.

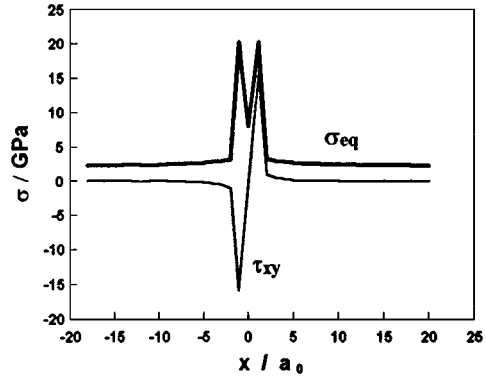

Figure 7 Equivalent Mises stress distribution in x direction at onset of plastic instability.

substrate plastic instability. Atomic trajectories show a complex pattern of atomic movements near the contact region: in (010) plane (Fig. 6a), atoms within a range of $5a_0$ in radius around the initial contact center move in a manner similar to the slip-line field in continuum plasticity, and atoms outside this semi-circle displace elastically in the radial directions. This atomic level displacement field is quite similar to that of Johnson's simple cavity model in elastic-plastic indentation of half-space [6]. However, atomic trajectories in (001) surface of the substrate (Fig. 6b) markedly demonstrate that atomic cross-layer movements along [010] direction also occur at the contact edges. To understand this non-plane-strain deformation mechanism, we plot atomic Mises equivalent stress $\sigma_{\rm eq}$ distribution at the surface in [100] direction, see Fig. 7. We find at onset of plastic instability, the maximum Mises stress along [100] occurs at the two side atoms just under the tip. This may be due to the significant contribution of large shear stress τ_{xy} to $\sigma_{\rm eq}$ (also plotted in Fig. 7) induced by the tip indentation. The value of $\sigma_{\rm eq}$ at side atoms is even greater than that at a point below the surface (see Fig. 4b). However, atoms with this maximum $\sigma_{\rm eq}$ at the contact edge does not "yield" in (010) surface, its strain energy is released through the cross-layer displacement in the [010] direction, suggesting that interstitial defects are generated. Nevertheless, our findings demonstrate that the material yielding at atomistic level in nanoindentation is still governed by the von Mises shear strain-energy criterion, and this yielding stress is significantly greater than the theoretical shear strength of ideal crystal lattice in two-dimensional cases [25], where for FCC copper, the value equals approximately to one sixth of the average shear modulus G, i.e., 9.1 GPa. Our simulations also demonstrate the temperature rise in plastic instability. The corresponding kinetic temperature increases from 0.1 K to 0.6 K due to the release of the substrate strain energy, then it comes back to the ambient temperature through the stochastic collisions via brownian dynamics.

Retraction of the tip reveals that the unloading curve is almost parallel to the loading one, resembling to the

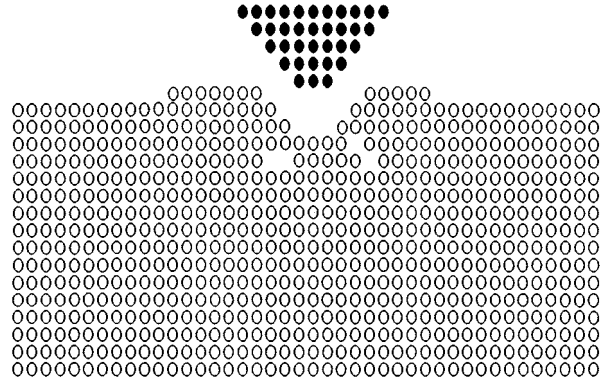

Figure 8 Atomic configuration of substrate defects after plastic indentation.

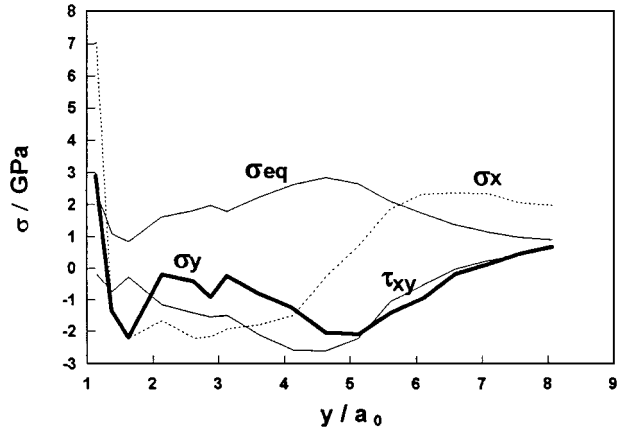

Figure 9 Atomic residual stress distributions on the *y* axis after plastic contact.

macroscopic behavior of an elastic-plastic bar under uniaxial loading and unloading cases, see Fig. 5a. Atomic trajectories (not depicted here) reveal that no cross-layer movements occur during this stage, suggesting that the material response during unloading is elastic. It should be noted that the potential energy (Fig. 5b) attains a minimum at about $1.3a_0$. At this point, the contact load is zero as a result of no bond stretching occurring between the two materials. Beyond this point, hysteresis occurs and the potential energy starts to increase, while the load becomes attractive until it reaches a maximum adhesion force (40 nN) at $0.5a_0$. This maximum value in hysteresis stage is much greater than that in elastic cases (comparing Fig. 1a and 5a), suggesting that the adhesion junction in plasticity is stronger than that in elastic case for pure metal contact. In the final stage of the tip separation, we observe that the adhesion force vanishes, and the system potential energy is greater than its initial value at onset of tip approaching. This indicates that defect energies are induced during the elasto-plastic indentation process.

Our refined investigations show that, as the tip is kept at the critical position of plastic instability, the spontaneous yielding process is accompanied by the atomic stress relaxations, the dramatic decreases in contact load and potential energy, the abrupt increase in kinetic temperature, and the atomic cross-layer movements along [010] direction (similar to that in Fig. 6b) and the pile-up of sample atoms in the vicinity of the tip. This unstable process proceeds over tens of picoseconds until no distinguished variations observed. The complexity of the material plasticity for FCC crystals may explain the macroscopic phenomenon where some ductile materials' elastic limits are greater than their yielding stresses, and our findings could also explain to some extent the micro-mechanisms of materials softening, such as rock material yield under compression.

Fig. 8 shows the atomic configuration after the tip separated from the substrate. Two adjacent (010) atomic slices are superimposed in order to see the substrate defects more clearly. These defects include subsurface vacancies, atomic steps on the surface and marked plastic indent. We do not observe dislocations generated in the substrate. This may be due to the fact that the deformation in nanoscale indentation is very localized and that the stored elastic energy is not sufficient to create this kind of defect. From the contact load and the projected area of the indent, we obtain the hardness of Cu being approximate 23 GPa, a value significantly larger than those in experiments for usual metals, and is even greater than that estimated from MD simulations at room temperature [5], indicating that the hardness of nanometer-scale material at low temperature is extremely high.

It is interesting to compare the residual stress distributions at atomistic level for plastic indentation with those of recent finite element method. Fig. 9 shows the residual stress distributions on the *y* axis. It can be seen that the normal stresses σ_x and σ_y are tensile at the surface, and compressive in the substrate within a range of $6a_0$, while the equivalent Mises residual stress σ_{eq} is relatively low. These results are quite similar to those in elastic-plastic finite element analysis of repeated microindentation of a half-space by a rigid sphere, where the sizes of the elements can be as small as 1.25 nm square [26].

4. Summary

A complete study on tip-to-substrate nanoindentation has been presented using the constant temperature and constant pressure molecular dynamics computer simulations. Emphases are placed on the characteristics of load-approach curve, the variations of the system potential energy, the atomic stress distributions, and the portraits of atomic trajectories and configurations.

Our main findings include:

1. For elastic indentation, the material's response is linear elastic during the loading-unloading cycle, except for the unstable JC phenomenon at the first contact and the hysteresis upon separation, which are accompanied by a rise in kinetic temperature. In particular, the maximum adhesive stress in hysteresis equals approximately to the Griffith theoretical fracture strength. Furthermore, the elastic disturbance is well within a few atomic layers, and the contact stress fields at atomistic level are comparable with those in the macroscopic Hertzian theory.

2. Of paramount importance is that the material yielding at atomic level is still governed by the von

Mises shear strain-energy criterion. The plastic instability is accompanied by the dramatic rise in kinetic temperature, the elastic-plastic displacements of atoms near the contact region, similar to those in Johnson's cavity model [6], and the cross-layer movements of atoms to release the high strain energy, suggesting that interstitial defects are generated during the nanoindentation.

3. Variations of the system potential energy in plasticity demonstrate that the defect energies are induced in plastic contact. These defects include substrate voids, surface steps and plastic indent. Line defects such as edge dislocations in the substrate are not observed.

Acknowledgements

This work is supported by the National Science Foundation (NSF) of China No. 59605005. The authors would also like to thank the State Key Laboratory of Tribology (SKLT), Tsinghua University and North China University of Technology for understanding and support to this work.

References

1. D. TABOR "The Hardness of Metals" (Clarendon Press, Oxford, 1951).
2. J. B. PETHICA, R. HUTCHINGS and W. C. OLIVER, *Philos. Mag.* **A48** (1983) 593.
3. "Handbook of Micro/Nano Tribology," edited by B. Bhushan (CRC Press, Boca Raton, FL, 1995).
4. K. KOMVOPOULOS, *Wear* **200** (1996) 305.
5. J. F. BELAK, D. B. BOERCKER and I. F. STOWERS, *MRS Bulletin* **18** (1993) 15.
6. K. L. JOHNSON "Contact Mechanics" (Cambridge University Press, 1985).
7. U. LANDMAN, W. D. LUEDTKE, N. A. BURNHAM and R. J. COLTON, *Science* **248** (1990) 454.
8. J. F. BELAK and I. F. STOWERS, in "Fundamentals of Friction," edited by I. L. Singer and H. M. Pollock (Kluwer, Dodrecht, 1992) NATO ASI Proceedings.
9. W. G. HOOVER, A. J. DE GROOT and C. G. HOOVER, *Phys. Rev.* **A42** (1990) 5844.
10. J. A. HARRISON, C. T. WHITE, R. J. COLTON and D. W. BRENNER, *Phys. Rev.* **B46** (1992) 9700.
11. H. RAFFI-TABAR, J. B. PETHICA and A. P. SUTTON, in Proceedings of MRS Symp., 1992, Vol. 239, p. 313.
12. M. S. DAW and M. I. BASKES, *Phys. Rev.* **B29** (1984) 6443.
13. R. A. JOHNSON, *Phys. Rev.* **B37** (1988) 3924.
14. B. WEI and K. KOMVOPOULOS, *Trans. ASME., J. Trib.* **118** (1996) 431.
15. S. M. FOILES, M. I. BASKES and M. S. DAW, *Phys. Rev.* **B33** (1986) 7983.
16. W. F. VAN GUNSTEREN and H. J. C. BERENDSEN, *Mol. Phys.* **45** (1982) 637.
17. Y. S. LENG, Y. Z. HU, L. Q. ZHENG and G. P. YANG, *Chinese J. Mater. Res.* **11** (1997) 267.
18. S. A. ADELMAN and J. D. DOLL, *J. Chem. Phys.* **64** (1976) 2375.
19. H. J. C. BERENDSEN and W. F. VAN GUNSTEREN, in Proc. Int. School of Physics <Enrico Fermi> (North-Holland, Amsterdam,1986) p. 43.
20. M. BORN and K. HUANG "Dynamical Theory of Crystal Lattices" (Clarendon Press, Oxford, 1954).
21. I. ALBER, J. L. BASSANI and M. KHANTHA, *Phil. Trans. Roy. Soc. Lond.* **A339** (1992) 555.
22. A. A. GRIFFITH, *ibid.* **A221** (1920) 163.
23. R. G. HOAGLAND, M. S. DAW, S. M. FOILES and M. I. BASKES, *J. Mater. Res.* **5** (1990) 313.
24. B. R. LAWN "Fracture of Brittle Solids," 2nd ed. (Cambridge University Press, 1993).
25. J. LUBLINER "Plasticiy Theory" (Macmillan Publishing Company, 1990).
26. E. R. KRAL, K. KOMVOPOULOS and D. B. BOGY, *Trans. ASME, J. Appl. Mech.* **60** (1993) 829.

Received 2 October 1997
and accepted 30 September 1999